Hydrogeology Journal (2015) 23: 533–550
DOI 10.1007/s10040-014-1216-z

Numerical modeling and environmental isotope methods in integrated mine-water management: a case study from the Witwatersrand basin, South Africa

Haile Mengistu · Abera Tessema · Tamiru Abiye · Molla Demlie · Haili Lin

Abstract Improved groundwater flow conceptualization was achieved using environmental stable isotope (ESI) and hydrochemical information to complete a numerical groundwater flow model with reasonable certainty. The study aimed to assess the source of excess water at a pumping shaft located near the town of Stilfontein, North West Province, South Africa. The results indicate that the water intercepted at Margaret Shaft comes largely from seepage of a nearby mine tailings dam (Dam 5) and from the upper dolomite aquifer. If pumping at the shaft continues at the current rate and Dam 5 is decommissioned, neighbouring shallow farm boreholes would dry up within approximately 10 years. Stable isotope data of shaft water indicate that up to 50 % of the pumped water from Margaret Shaft is recirculated, mainly from Dam 5. The results are supplemented by tritium data, demonstrating that recent recharge is taking place through open fractures as well as man-made underground workings, whereas hydrochemical data of fissure water samples from roughly 950 m below ground level exhibit mine-water signatures. Pumping at the shaft, which captures shallow groundwater as well as seepage from surface dams, is a highly recommended option for preventing flooding of downstream mines. The results of this research highlight the importance of additional methods (ESI and hydrochemical analyses) to improve flow conceptualization and numerical modelling.

Keywords Numerical modeling · Dykes · Mine shaft · Tritium · South Africa

Received: 17 April 2014 / Accepted: 20 November 2014
Published online: 20 December 2014

Electronic supplementary material The online version of this article (doi:10.1007/s10040-014-1216-z) contains supplementary material, which is available to authorized users.

H. Mengistu (✉)
Wayne County Community College District,
801 W Fort Street, Detroit, MI 48226, USA
e-mail: hrmengistu@gmail.com

A. Tessema
Department of Geology,
University of Limpopo, Turfloop Campus,
Private Bag X1106, Sovenga, 0727, South Africa
e-mail: tessemaabera@gmail.com

T. Abiye
School of Geosciences,
University of the Witwatersrand,
P/Bag 3, WITS, 2050, Johannesburg, South Africa
e-mail: tamiru.abiye@wits.ac.za

M. Demlie
School of Geological Sciences,
University of KwaZulu-Natal,
Private Bag X54001, Durban, South Africa
e-mail: demliem@ukzn.ac.za

H. Lin
Council for Geoscience,
280 Pretoria Street, Pretoria, 0001, South Africa
e-mail: hjia@geoscience.org.za

Introduction

Conventional numerical models are designed to simulate idealized field scenarios whereby the most reliable outcome is obtained if most of the assumptions are partially or fully met (Mills et al. 2002; Swanson and Bahir 2004; Chiang 2005; Voss 2011a, b). When real field situations entail increasingly far from ideal assumptions, uncertainties of model outcomes become so significant as to make the results unacceptable. While parameter estimation and optimization codes now facilitate a greater ability to reduce model parameter uncertainty, and aid model calibration, a robust conceptual model is the fundamental basis for successful numerical modelling. Environmental stable isotope (ESI) and hydrochemistry data analyses can be used to assist in developing such a conceptual model, providing input to allow improved numerical modelling (Ji-Chun and Xian-Xi 2013; Keating et al. 2010).

ESIs of oxygen ($\delta^{18}O$) and hydrogen ($\delta^{2}H$) are commonly used to develop conceptual groundwater flow paths, to identify recharge/discharge areas, mixing processes and salinization, and to understand evolution of

groundwater flow (Aravena 1995; Pulido-Bosch et al. 1997; Larsen et al. 2001; Schofielda and Jankowski 2004; Huang and Chen 2012). Careful analysis of ESI records elucidate evaporation and condensation processes, and when the data are used along with site information, an improved conceptualization of groundwater flow can be realized with reasonable confidence (Dotsika et al. 2010). Moreover, water mixing and possible flow paths can be understood by assessment of selected inorganic chemical constituents (Mazor 1997).

Stilfontein, a small mining town, is situated at roughly 300 km west–south-west of Johannesburg in the North West Province of South Africa (Fig. 1). The region represents the farthest western extension of the greater Witwatersrand gold-bearing horizons, locally identified as reefs (SACS 1980). The Margaret shaft, located at the eastern margin of Stilfontein town, is situated in the Klerksdorp-Orkney-Stilfontein-Hartebeestfontein (KOSH) gold mining area. The shaft, constructed in 1949, was as one of four shafts at the Old Stilfontein Gold Mine. All underground mining activities in Stilfontein area stopped in 1992 triggering complete and partial demolition of all but Margaret shaft, which has been used since then for controlling water from flooding downstream mines by means of the two major pumps situated at approximately 650 m below ground level (bgl) and 950 m bgl. Between 2008 and 2010, the volume of fissure water reaching the Margaret shaft significantly increased by approximately 5,000 m^3/day (T. Else, Manager of Margaret Water Company, personal communication, 2010). Within the lower reaches of the Koekemoer Catchment, southeast of Margaret Shaft, a second pumping shaft, namely Eastern Shaft, was also pumping at a rate of roughly 6,000 m^3/day in 2010.

Water flow and pollution investigations were conducted previously by private consultants mainly to address specific issues, initiated and funded by the mining companies (Veltman and Wilke 2008, unpublished data). Given the uncertainty of conclusions derived from the use of many tools, including numerical models and geochemical studies in fractured, karstic and mined-out areas, there has been a need to conduct broad-based study to thoroughly understand the groundwater dynamics on a catchment level and to use additional methods to validate and evaluate the accuracy of results from the various tools (Konikow and Bredehoeft 1974).

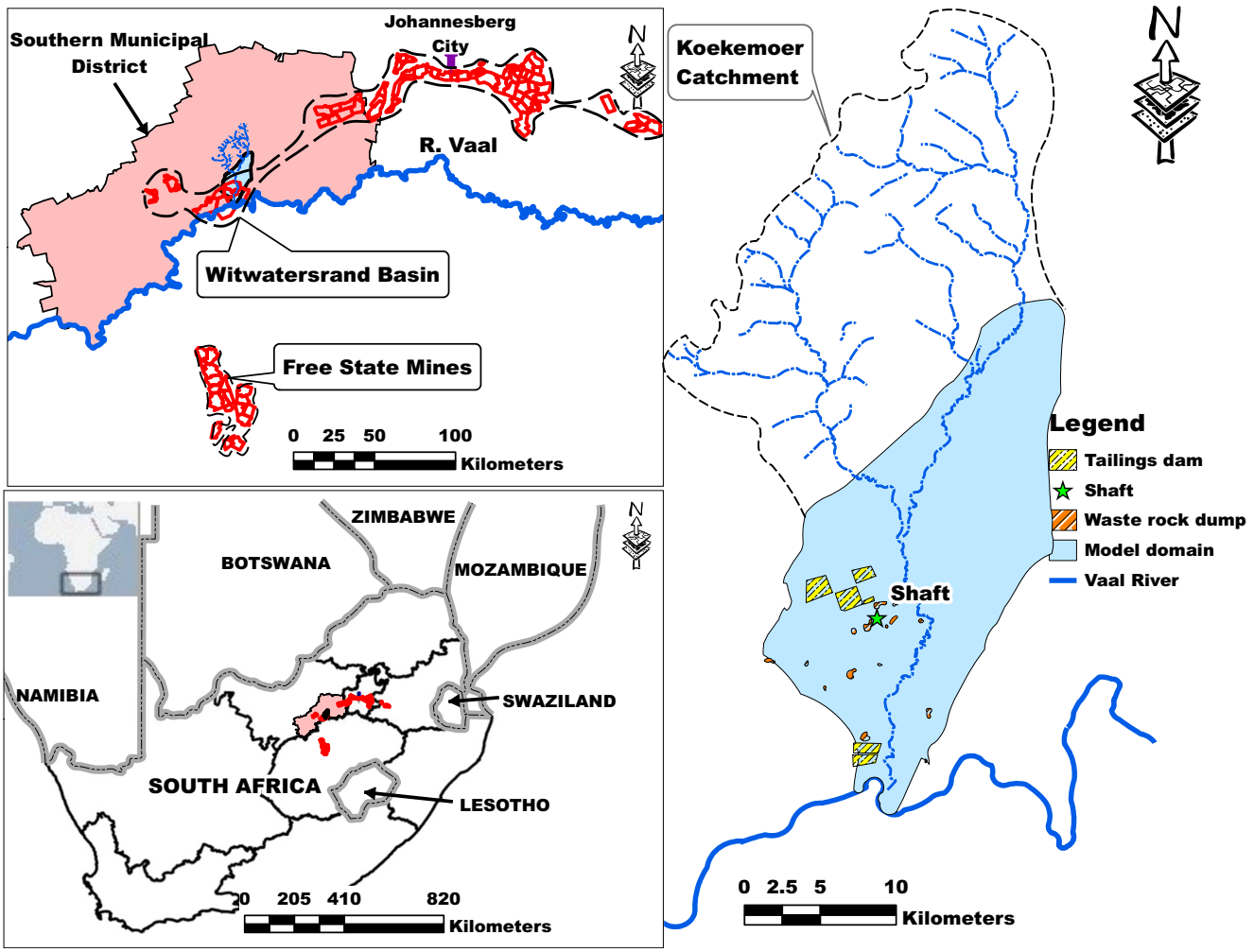

Fig. 1 Location map of the study area

DOI 10.1007/s10040-014-1216-z

The current investigation arose from the need to address the problem of sudden increase of water flow to the dewatering shafts, through improved understanding of the conceptual flow model and updating the existing numerical model (completed few years ago) by incorporating new developments. The results of numerical simulation, based on improved flow conceptualization using ESI and hydrochemical results, are collated to build a platform that provides accurate and relevant information on subsurface water flow, thereby supporting any judgement on whether the present integrated mine-water management scheme is the best option.

Site physiographic background

The Koekemoer Catchment, with an area of about 650 km^2, is bounded by Schoonspruit Catchment in the west, Kromdraispruit Catchment in the east and the Vaal River in the south. The major mining area including Margaret Shaft lies in the bottom quarter of the Koekemoer Catchment. The Koekemoer Stream, flowing from north to south, is a tributary of the westerly flowing Vaal River, which coincides with the southern tip of the model area (Fig. 1).

The highest topographic elevation is situated in the northern portion of the area reaching roughly 1,550 m above mean sea level (amsl), whereas the lowest elevation of approximately 1,290 m amsl is located at the confluence of the Koekemoer Stream and the Vaal River (DWA 2006). The landform is characterized by slightly undulating to flat topography with less than 30 m elevation difference in the E–W direction over a distance of approximately 10 km, whereas the general elevation difference is roughly 260 m over 11 km along the N–S strike (Fig. 2). The drainage pattern is dendritic mainly because of the lack of prominent surface structures and the lithology of the surrounding rocks.

Geologic and hydrogeologic setting

The geology of the area is dominated by Transvaal dolomites (Malmani Subgroup) of Archaean age underlain by a thin, steeply dipping Transvaal Quartzite unit, flanked by the Ventersdorp volcanics and sediments, which is

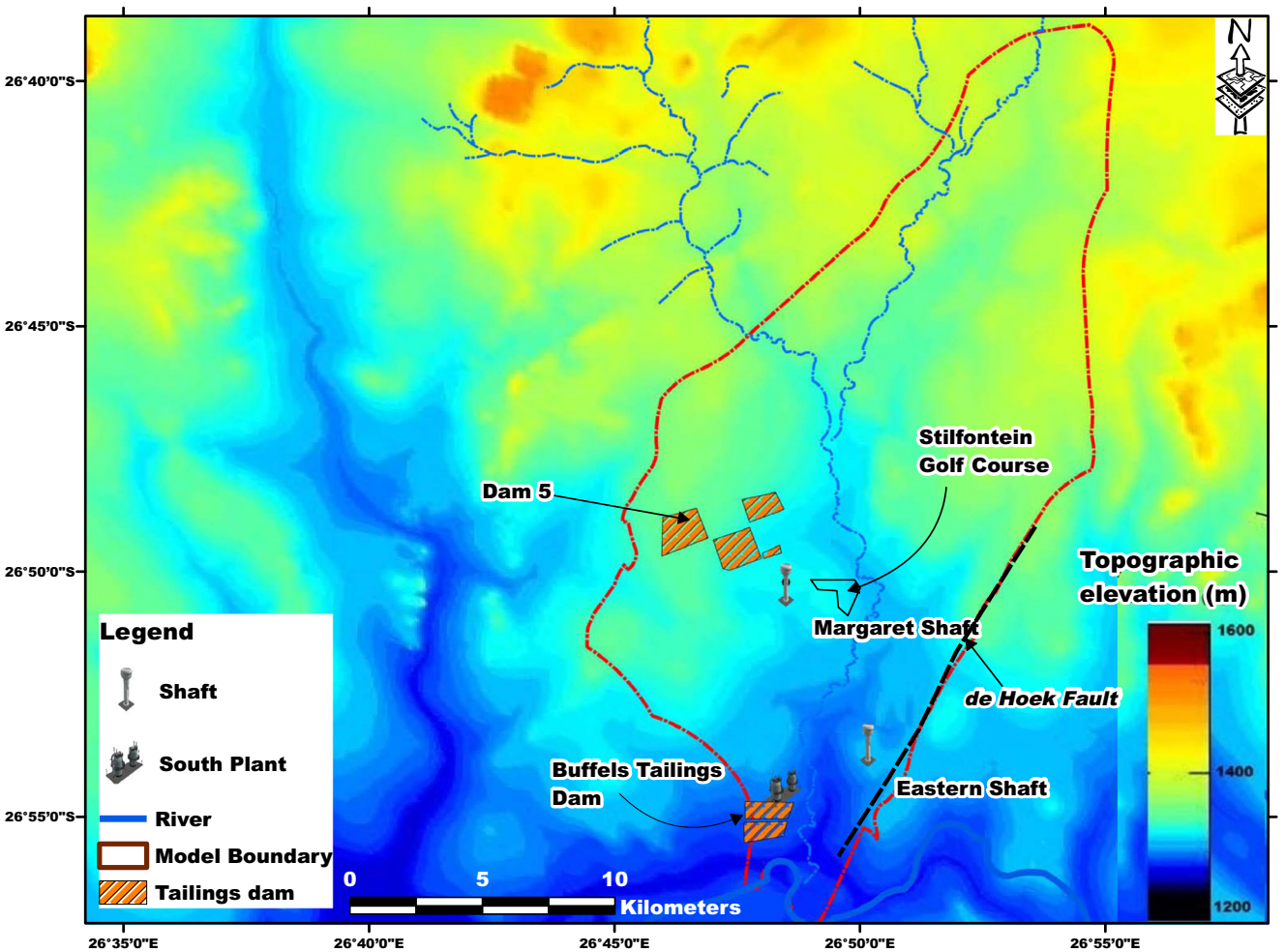

Fig. 2 Study area topographic elevation map with relevant features (tailings dams, seepage dams, boundaries and structures)

 DOI 10.1007/s10040-014-1216-z

comprised of bimodal volcanic and siliciclastic sedimentary rocks (Eriksson et al. 2006; Van Niekerk and van der Walt 2006; Prinsloo 2007; Tessema et al. 2012). The lower most sequence is the Witwatersrand Supergroup consisting of fluvial and shallow-marine sedimentary rocks (quartzites and shale) and described as the most important gold-bearing formation (Naickera et al. 2003; Fig. 3). Except at flood plains of the Koekemoer Stream, soil development is fairly poor as well as full of chert grits due to weathering of dolomites with chert intercalation (Abiye et al. 2011). Winde and van der Walt (2004) reported that where the dolomite is chert-poor, the soil tends to be fine sandy-loam, whereas clay rich soils are common in matured floodplains of the Koekemoer Stream and Vaal River.

Two aquifers, namely the upper highly weathered and karstified dolomite and the lower slightly weathered and fractured Malmani dolomite, constitute the most important water-bearing units in the area. The Malmani dolomite is compositionally heterogeneous in that in some sections it is chert-rich (locally named the Oak-Tree Formation), varying laterally to be chert-poor (known as Monte-Christo Formation; Smith and Ritzi 1993; Yager and Kappel 1998; Kafri and Foster 1989). The intercalation of chert layers within the dolomite geology in the region plays a major role in groundwater storage and flow; chert-rich dolomite units exhibit higher transmissivity and chert-poor dolomites are known to have subdued transmissivity (Veltman and Wilke 2008). Two systems of dykes are also situated in the study area; Kimberlite Dyke with mafic to ultramafic composition, and Pilansberg dykes with alkaline composition (Veltman and Wilke 2008). Kimberlite Dykes are reported to enhance flow and storage of groundwater, whereas Pilanesberg dykes with no prominent fracturing impede groundwater flow (McCarthy 2006; Fig. 4). Quaternary alluvial sediments of small aerial extent are evident along the lower reaches of the Koekemoer Stream and the Vaal River (Veltman and Wilke 2008).

Water level data in several monitoring boreholes suggest that groundwater flow in the upper weathered

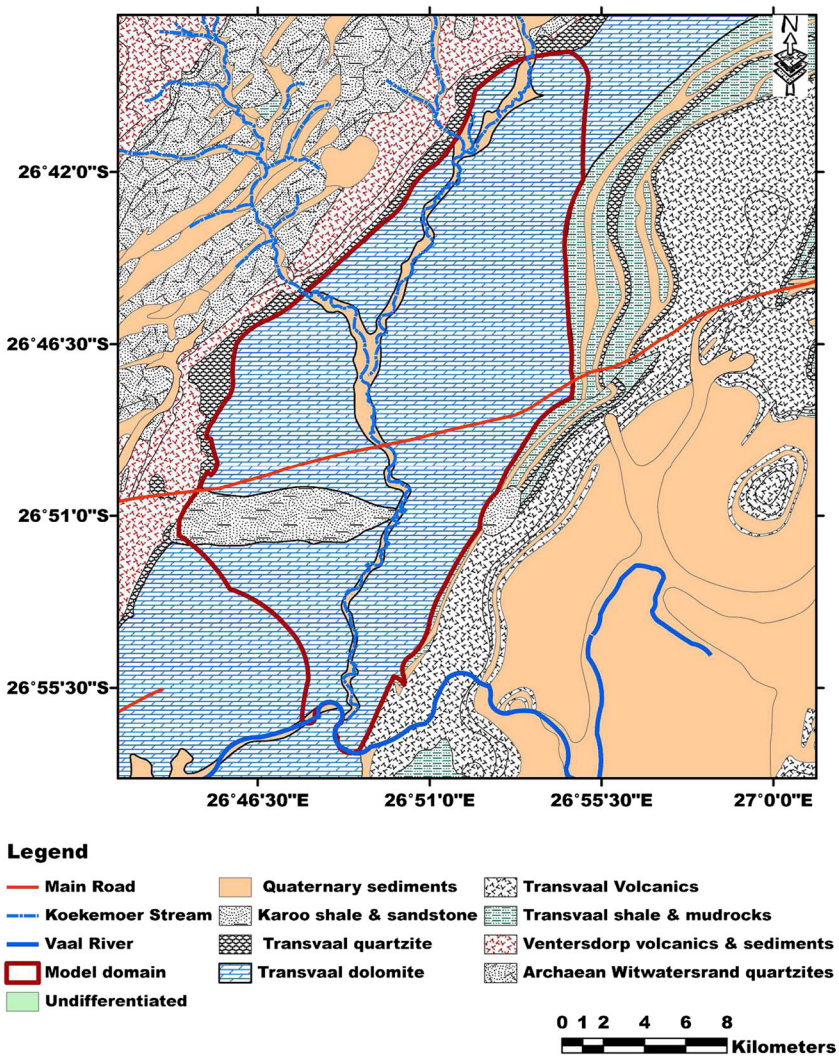

Fig. 3 Simplified geological map of the project area (Simplified from 1:250,000 geological map of West Rand, Dept. of Mineral and Energy Affairs 1986)

 DOI 10.1007/s10040-014-1216-z

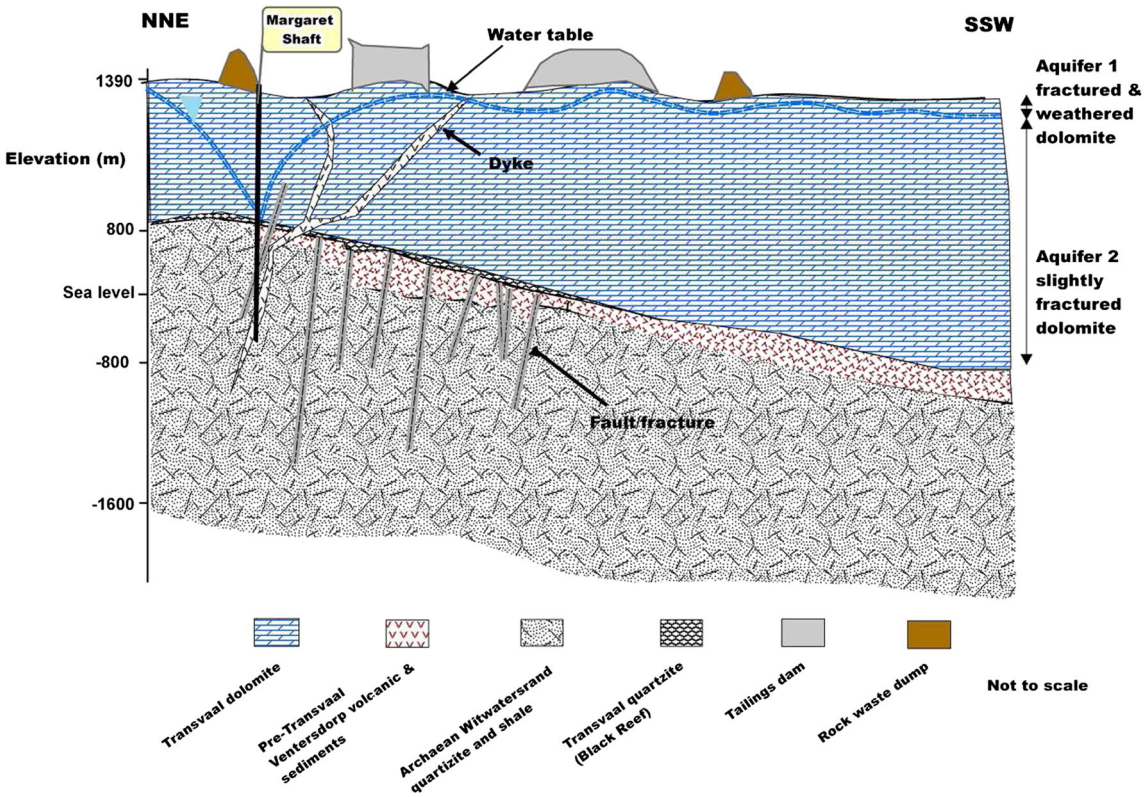

Fig. 4 Simplified geological section of the project area from NNE to SSW. The elevations are in meters above or below mean sea level

aquifer follows the topography towards the south in the direction of the Vaal River. On the other hand, groundwater movement within the deeper dolomite aquifer is associated with N–S trending joints and faults and flow takes place towards the Vaal River and points of abstraction such as Margaret and Eastern Shafts (Winde and Van der Walt 2004).

According to Winde and van der Walt (2004), mean annual recharge ranges from 4 to 6 % of the mean annual precipitation, which is 650 mm, and evaporation is estimated to be about 2 m based on Class A pan measurement. Evidence of poor and mature soil development in various areas and flood plains of the Koekemoer Stream/Vaal River respectively as well as relatively flat topography contribute to spatially variable recharge rates in pre-mining condition (Winde and van der Walt 2004).

Methodology

Pumping tests were conducted at five different sites, each using a pipe of 80-mm inner tube diameter and 80-m long 20-KWa skid mount generator pump with AquaMaster™ electronic flow meter and Solinist™ Model 3001 water level logger. The tests were conducted for 48 h of pumping and 12 h of recovery and water level data were transferred electronically to a memory key. Calculation of aquifer parameters (transmissivity and storage coefficient) was done with AQTESOLV pro™ software.

Groundwater and surface water samples were taken during the dry season (June–August) using 250-ml HDPVC bottles in triplicate for a site (one sample was acidified with 10 % HNO_3 and filtered, the second sample was unfiltered and not acidified, and the third sample was acidified but not filtered). Samples were properly labelled and stored in portable cool boxes at 4 °C until submission to the laboratory. Field duplicates and blank samples were also taken one every 10 sites. Cation analyses were performed using a Perkin Elmer ELAN® DRC II ICP-MS system that was calibrated according to the manufacturer's specification, whereas anions were measured using a Dionex® ion chromatograph (IC) analytical system with US EPA method 300.1.

Water samples taken during June–August for ESI analyses, were retained in 1-L HDPVC bottles and were transferred to portable cool boxes and stored at 4 °C. Sampling was intentionally conducted 11 AM–2 PM to reduce d-excess, which is considered as a reliable tracer of variations in atmospheric moisture (Farlin et al. 2013). Samples were taken from boreholes, seepage dams, Vaal River, Koekemoer Stream and from four various depths in the Margaret shaft: level-3 or 180 m bgl, level-5 or 350 m bgl, level-10 or 650 m bgl and level-16 or 960 m bgl.

Water $^{2}H/^{1}H$ and $^{18}O/^{16}O$ ratios were analysed in the laboratory of the Environmental Isotope Group (EIG) of iThemba Laboratories, in Johannesburg, South Africa. The equipment consists of a PDZ Europa GEO 20–20 gas mass–spectrometer connected to peripheral sample

DOI 10.1007/s10040-014-1216-z

preparation devices. A PDZ water equilibration system (WES) was employed for hydrogen and oxygen isotope analysis according to Schimmelmann and DeNiro (1993), and equilibration for oxygen done according to the procedure of Socki et al. (1992). Analytical results are presented in the common delta-notation with measurement precision estimated at 0.1 ‰ for oxygen and 0.5 ‰ for hydrogen. Delta values are expressed as per mil relative to a known standard, in this case standard mean ocean water (SMOW) for $\delta^{18}O$ and $\delta^{2}H$.

Tritium analysis was done by a low-level liquid scintillation spectrometer, with 500 ml of the water sample, according to the protocol developed by International Atomic Energy Agency (IAEA) and USEPA Method 906. For liquid scintillation counting, samples were prepared by directly distilling the enriched water sample from the highly concentrated electrolyte, with a detection limit of 0.2 TU.

Processing MODFLOW for WINDOWS (PMWIN), a quasi three-dimensional (3D) finite difference computer algorithm developed by Harbaugh et al. (2000), was used for numerical modelling (Chiang 2005). A fundamental assumption of MODFLOW is that the hydrogeological units represented by model layers are composed of continuous porous media.

Groundwater flow conceptualization

Current groundwater head data demonstrate that the general groundwater and surface water flow direction is southerly towards the Vaal River, and there is evidence that there is groundwater flow towards the Margaret and the Eastern Shafts from the surrounding areas as well as easterly and westerly local flows towards the Koekemoer Stream. Groundwater flow conceptualization is refined by ESI and hydrogeochemical information.

Environmental stable isotopes

Interpretation of ESI data can be carried out using the meteoric line derived from long-term records of stable isotope data for rainfall with relatively similar climate, geography and location (Craig 1961; Harris et al. 2010). Samples were collected from shallow boreholes, deep boreholes (at various shaft depths), a stream, a river and the seepage from Dam 5. Geographically, the sample sites are distributed around the Margaret shaft and include the upstream area in the northern part of the study site and the downstream area in the south as far as the Vaal River (Fig. 5).

ESI data of the area show that $\delta^{18}O$ ranges between −4.3 and 1.1 ‰, while $\delta^{2}H$ ranges from −26.5 to 7.6 ‰. The most enriched samples (1.1 ‰ for $\delta^{18}O$ and 7.6 ‰ for $\delta^{2}H$) represent evaporating surface water of Dam 5, whereas values of −4.3 ‰ and −26.5 ‰ for $\delta^{18}O$ and $\delta^{2}H$ respectively signify the most depleted shallow groundwater situated west and north of Dam 5. Almost all ESI data for groundwater samples, except the most depleted western and northern areas, fall below the global meteoric water line (GMWL) showing that the waters underwent enrichment due to isotope fractionation caused by evaporation during or before recharge (Fig. 6). Relative depletion of ESIs in groundwater in the western and northern areas imply (qualitatively) possible bypass recharge of episodic heavy precipitation and the absence of considerable mixing with highly evaporated surface waters, but less of a likelihood of recharge at higher altitude, considering the size of the Koekemoer catchment. According to Gibson et al. (1993), any measurable enrichment of groundwater does not occur without mixing with evaporated surface water bodies. All other water samples lie between the two extremes; that is between Dam 5 and the northern farm boreholes and boreholes west of Dam 5 (Fig. 6).

The relatively more enriched isotope data of level-10 (MSL-10), compared with shallow levels, most likely suggest that a high proportion of water originating from surface seepage is mixing through a network of tunnel connections in the old mine. At other levels, at 350 m bgl (MSL-5) and at approximately 180 m bgl (MSL-3), there are no direct conduits to the Margaret shaft and therefore the samples show slightly more depleted value than the sample at 950 m bgl. The result is consistent with similar studies elsewhere in the greater Witwatersrand Basin where underground mining activities cause deep infiltration of meteoric water along a number of haulages and natural horizontal fractures (Duane et al. 1997).The upstream Koekemoer Stream samples are clustered in the central part of the graph (Fig 6) showing a mixture of the depleted western shallow groundwater with the shallow groundwater located north of Dam 5 and surface water infiltrating from Dam 5.

The data plot (Fig. 6) shows that all deep water samples from various shaft levels are close in their ESI composition to northern and western borehole waters suggesting that water contribution from the shallow aquifer is proportionally higher than seepage water from Dam 5 and other surface water bodies. On the other hand, the ESI signature of the middle Koekemoer Stream samples resembles the MSL-3 and MSL-5 samples signifying the discharge of excess water from Margaret Shaft into the stream especially during the dry winter.

Where sufficient local rainfall ESI data are absent to construct a representative local meteoric water line (LMWL), the global meteoric water line (GMWL) is often a satisfactory benchmark for determining likely rainfall ESI compositions. Considering the close match between the GMWL and the majority of the groundwater ESI data (western and northern boreholes) and the progression with which surface waters diverge from the GMWL, it is reasonable to argue that meteoric water recharges the shallow groundwater without undergoing evaporation. The data show that samples whose ESI compositions are close to the GMWL (western and northern groundwater) represent one end member, whereas the seepage water from Dam 5 is considered as the other extreme end member. The ESI signature of all

 DOI 10.1007/s10040-014-1216-z

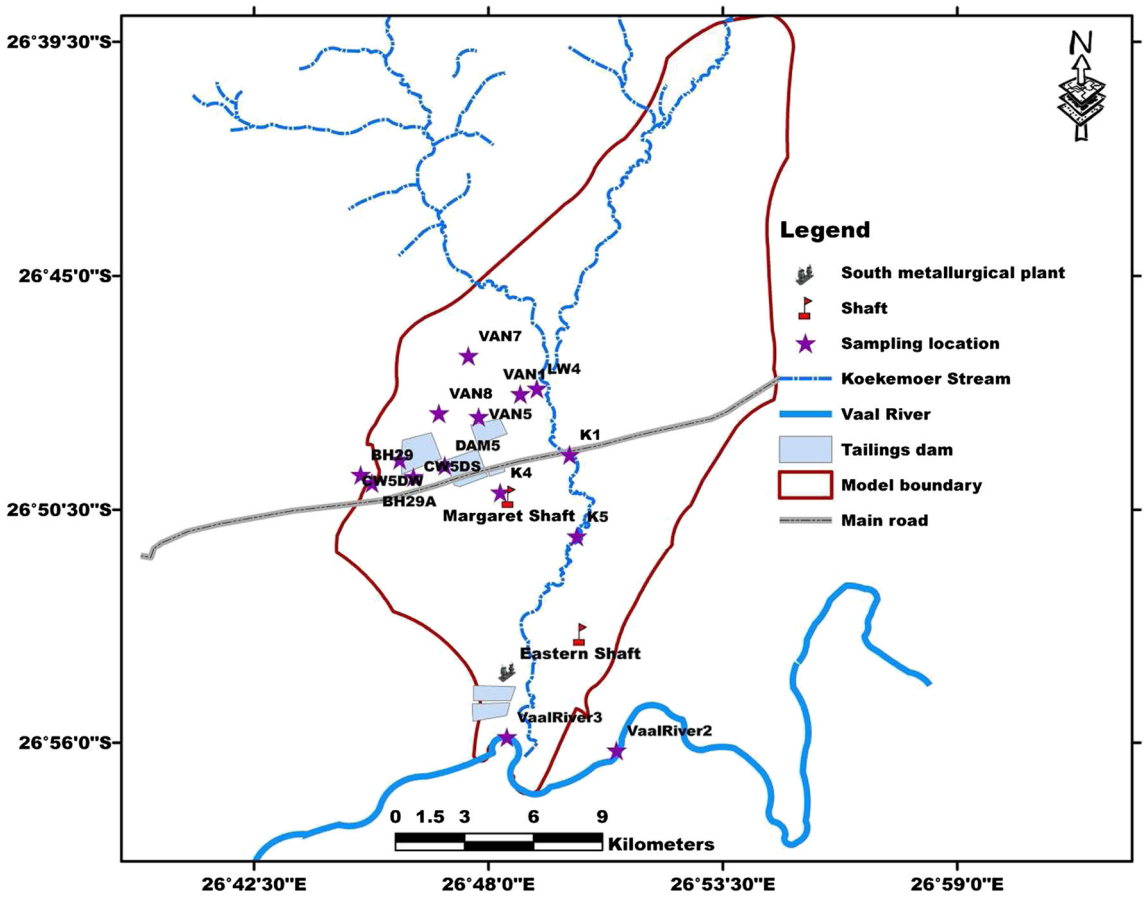

Fig. 5 Isotope sample locations, along with major physiographic landmarks

samples including the shaft water samples at the three levels, which lie in between the two extremes, suggest mixing of groundwater with close adherence to the GMWL and surface water bodies. Semi-quantitative mixing estimations were done (Eq. 1) to evaluate the contribution of precipitation with and without evaporation using end-member ESI compositions (Mazor 1997):

$$\%\ \text{Surface water} = \frac{(\delta D_{GMWL} - \delta D_{measured})\text{sample}}{(\delta D_{GMWL} - \delta D_{measured})\text{Dam5}}\ \text{X}\ 100\% \quad (1)$$

where

δD_{GMWL} sample=calculated sample δD value using GMWL equation
$\delta D_{measured}$ sample=measured sample δD value
δD_{GMWL} Dam 5=calculated Dam 5 δD value using GMWL equation
δD_{GMWL} Dam 5=measured Dam 5 δD value

Poor correlation (roughly 20 %) was calculated when monthly average precipitation was plotted against $\delta^{18}O$ demonstrating that amount effect or rainout effect does not cause noticeable variation in isotope composition of the study area—see electronic supplementary material (ESM). The result shows that the ESI composition of incoming water vapour from the source significantly varies when it reaches the study area (Lee and Fung 2007). Seasonality is also not important in this scenario because sampling was conducted within one season and at a similar time of the day. Altitude effect was estimated with reference to previous work by Harris et al. (2010) in the Table Mountain area of Cape Town, South Africa. The estimation, although relatively small compared to a study by Poage and Chamberlain (2001), was used to calculate the potential error introduced to the measured isotope data. Inclusion of the altitude effect in the error calculation is justifiable because of its site specificity (Gat et al. 2001). Margin of error was calculated using:

1. The error related to the laboratory method: $\delta^{18}O$=0.1 ‰ and δD=0.5 ‰
2. Altitude effect (adapted from Cape Town area): $\delta^{18}O$=0.22 ‰ and δD=1.4 ‰

Total margin of error: $\delta^{18}O$=0.31+0.1=0.32 ‰ and δD=0.5+1.9=2.4 ‰.

The percentage of surface-water mixing was calculated using the western boreholes and seepage water from Dam 5 as groundwater and surface-water end members,

DOI 10.1007/s10040-014-1216-z

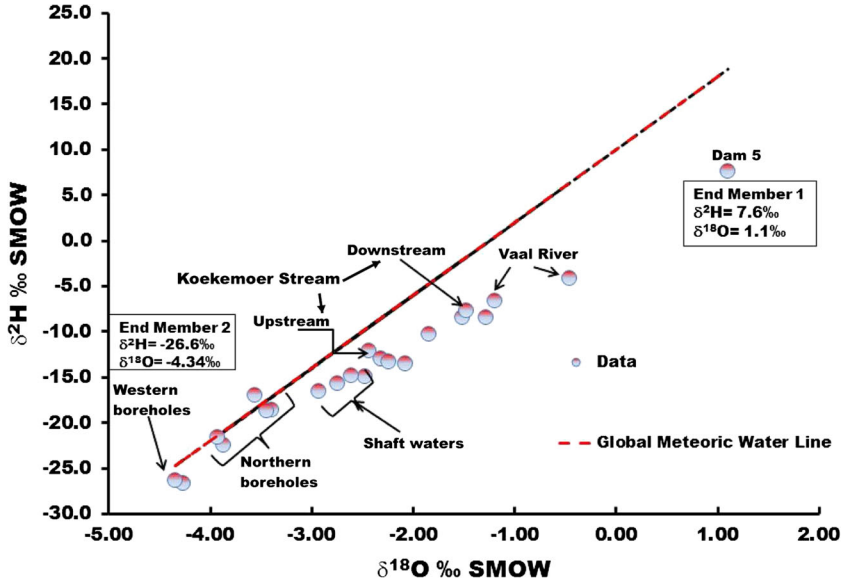

Fig. 6 Stable isotope data plot. The upstream and middle parts of Koekemoer Stream as well as shaft water samples cluster in the central area; western and northern boreholes cluster in the *lower left* (depleted) portion with Vaal River; downstream of Koekemoer Stream and Dam 5 samples spreading to the enriched *upper right corner* of the figure. Notice the close clustering of shaft and upper as well as middle Koekemoer Stream samples

respectively; the water samples taken at the four shaft levels ranged from 33.0±1.0 % to 49.6±0.8 % surface water (Table 1). The northern boreholes' surface-water content ranged between roughly 1 and 14 %, indicating a fast recharge process of meteoric water without substantial evaporation (Table 1).

Evaporation is assessed through comparing ESI data for surface waters with the global meteoric water line (Mazor 1997). The calculated slope of the evaporation line is 5.75 with an intercept of 0.17, lower than the GMWL slope of 8. The data demonstrate that the current climate in the region is causing severe evaporation of surface water owing to very low air moisture, leaving relatively enriched ESI signatures with respect to the global meteoric lines (Fig. 7).

Table 1 Measured environmental isotope data of $\delta^{18}O$ (‰) and $\delta^{2}H$ or δD (‰), δD_{GWML} representing calculated δD using the GMWL equation with measured $\delta^{18}O$ as input. Estimated percentage of surface water in all samples, with margin of error calculated using the mixture formula (Eq. 1). All uncertainties associated with the laboratory method and errors introduced due to altitude effect were incorporated in the calculation of margin of error

Sample location	Sample ID	δD (‰)	$\delta^{18}O$ (‰)	δD_{GMWL} (‰)	Percent surface water (%)	Margin of error (%)
Western boreholes	BH29	−26.61	−4.26	−24.11	22.4	±1.1
	BH29A	−26.28	−4.34	−24.74	13.8	±1.2
Shaft samples						
180 m bgl	MSL-3	−14.91	−2.48	−9.83	45.4	±0.8
350 m bgl	MSL-5	−14.82	−2.61	−10.91	34.9	±1.0
650 m bgl	MSL-10	−10.31	−1.84	−4.75	49.6	±0.8
950 m bgl	MSL-16	−15.69	−2.75	−11.99	33.0	±1.0
Northern boreholes	VAN1	−22.49	−3.87	−20.93	13.9	±1.3
	VAN5	−18.59	−3.40	−17.18	12.6	±1.3
	VAN7	−18.65	−3.44	−17.53	1.0	±1.3
	VAN8	−21.55	−3.93	−21.44	0.9	±1.4
Koekemoer Stream (upstream – downstream)	K4	−16.53	−2.93	−13.45	27.7	±1.1
	K1	−13.54	−2.08	−6.65	65.6	±0.6
	K5	−13.29	−2.24	−7.93	47.8	±0.8
Stilfontein Bullet Factory	LW4	−12.93	−2.32	−8.56	39.4	±0.9
Vaal River	VAAL2	−4.11	−0.46	6.32	93.1	±0.2
	VAAL3	−6.59	−1.20	0.42	62.6	±0.6
Stilfontein Dam	DAM5	7.60	1.10	18.80	100.0	±0.1

MSL Margaret Shaft level; *m bgl* meters below ground level

DAM5, *K1*, *K4*, *K5*, *VAAL1* and *VAAL2* are surface water samples. δD_{GWML} denotes δD calculated using sample $\delta^{18}O$ with the GWML equation: $\delta D = 8\delta^{18}O + 10$

 DOI 10.1007/s10040-014-1216-z

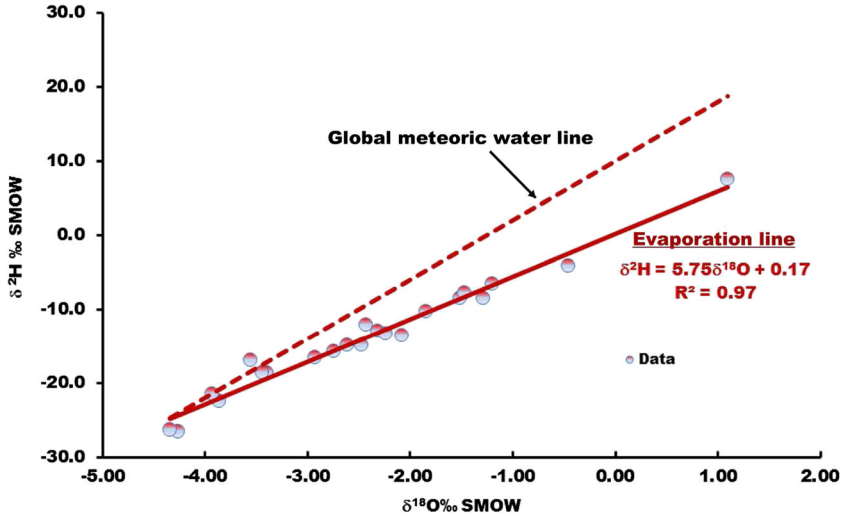

Fig. 7 Local area evaporation line of surface waters using $\delta^{18}O$ and δD values. The calculated slope of the evaporation is 5.75 with an intercept of 0.17, lower than the global meteoric water line slope of 8

Hydrogeochemical data

Hydrochemical analyses were done for groundwater and surface-water samples located systematically upstream and downstream of the shaft to assess the hydrochemical variability and the processes responsible for the chemical footprint as well as the mixing of waters of various origins (Table 2).A Piper diagram (Fig. 8) shows that there are three groups of similar water chemistry; Ca–Mg–SO_4-type, Ca–Mg–HCO_3 and Ca–Mg–SO_4–HCO_3-type waters. It is evident that the Ca–Mg–HCO_3-type water originates from areas situated north of Dam 5, whereas the source of Ca–Mg–SO_4-type water is seepage from Dam 5. From the identified groundwater flow and surface-water flow directions, it is apparent that waters of Ca–Mg–HCO_3-type chemical signature represent the most upstream sites situated in the northern portion of the area. On the other hand, Ca–Mg–SO_4-type waters, from areas located south and downstream of Dam 5, indicate signature of water chemistry presumably emanating from the mining dumps (Hodgson et al. 2001). Therefore, the intermediate Ca–Mg–SO_4–HCO_3-type water chemistry is thought to be a mixture of the two water-chemistry end members. The bulk hydrochemical data are indicative of the dominating carbonate geology modified by mixing with seepage water from local mine dumps.

The ESI data and the hydrochemistry data show that Ca–Mg–SO_4-type water is represented by highly enriched water, which implies that the highly polluted water,

Table 2 Major ion data with field-measured parameters (*pH* and *EC*) of surface water and groundwater samples

Sample ID	EC (mS/m)	pH	TDS (mg/L)	M Alk ($CaCO_3$) (mg/L)	Ca^{2+} (mg/L)	Cl^- (mg/L)	Mg^{2+} (mg/L)	Total NO_3^- (mg/L)	K^+ (mg/L)	Na^+ (mg/L)	SO_4^{2-} (mg/L)
BH29	22.27	7.61	170.50	98.50	21.57	7.56	9.50	1.58	2.00	11.11	8.94
BH29A	37.22	7.49	236.86	169.57	42.21	5.81	14.86	5.46	2.00	12.85	7.92
CW5DW	439.28	7.43	3915.50	206.11	469.72	175.09	253.24	1.10	8.61	326.83	2649.60
CW5DS	442.29	7.48	4199.36	220.64	479.57	178.70	246.71	7.95	6.19	333.79	2557.00
K4	169.63	8.21	1412.00	220.38	139.81	63.55	91.63	1.14	3.75	114.06	685.20
LW4	90.65	7.71	679.38	339.23	73.46	49.88	58.77	1.50	23.54	85.63	125.40
K1	80.59	8.16	633.14	222.13	71.00	16.00	52.03	0.50	3.33	41.50	105.00
K5	63.37	8.27	514.60	252.38	57.13	13.05	47.81	0.80	3.90	21.63	133.00
VAN1	63.64	7.87	405.00	235.21	69.78	8.30	50.97	ND	1.86	4.87	66.00
VAN5	64.82	7.49	412.50	347.01	75.75	4.90	48.44	ND	1.79	4.34	67.00
VAN7	62.07	8.09	395.00	247.46	67.01	4.70	52.59	ND	1.92	4.68	63.00
MSL-3	267.07	8.15	1960.50	145.40	205.90	85.50	118.70	ND	6.50	163.10	1006.50
MSL-5	247.80	7.90	1819.00	189.10	154.70	72.00	95.20	ND	6.10	218.40	942.00
MSL-10	67.50	8.10	568.50	256.20	141.40	16.50	80.40	ND	4.20	91.50	241.50
MSL-16	57.20	8.45	461.50	317.20	45.80	22.00	28.50	ND	2.30	67.60	176.50
VAAL2	64.56	8.63	450.00	110.00	49.64	55.04	21.68	1.81	12.17	62.95	97.00
VAAL3	118.82	8.26	2911.00	102.00	390.67	88.13	113.10	1.87	32.46	231.29	1757.00

M Alk total alkalinity (exclusively from carbonates within samples pH range, 7.43–8.63); *ND* below detection limit

BH29 and *BH29A* are boreholes west of Dam 5 (western boreholes); *K1*, *K4* and *K5* are Koekemoer Stream samples, whereas *VAAL2* and *VAAL3* are Vaal River samples; *VAN1*, *VAN5* and *VAN7* are shallow boreholes north of Dam 5 (northern boreholes); *CW5DW* and *CW5DS* are boreholes in the immediate vicinity of Dam 5; *MLS-3*, *MLS-5*, *MLS-10* and *MLS-16* represent samples from Margaret Shaft at various depths

 DOI 10.1007/s10040-014-1216-z

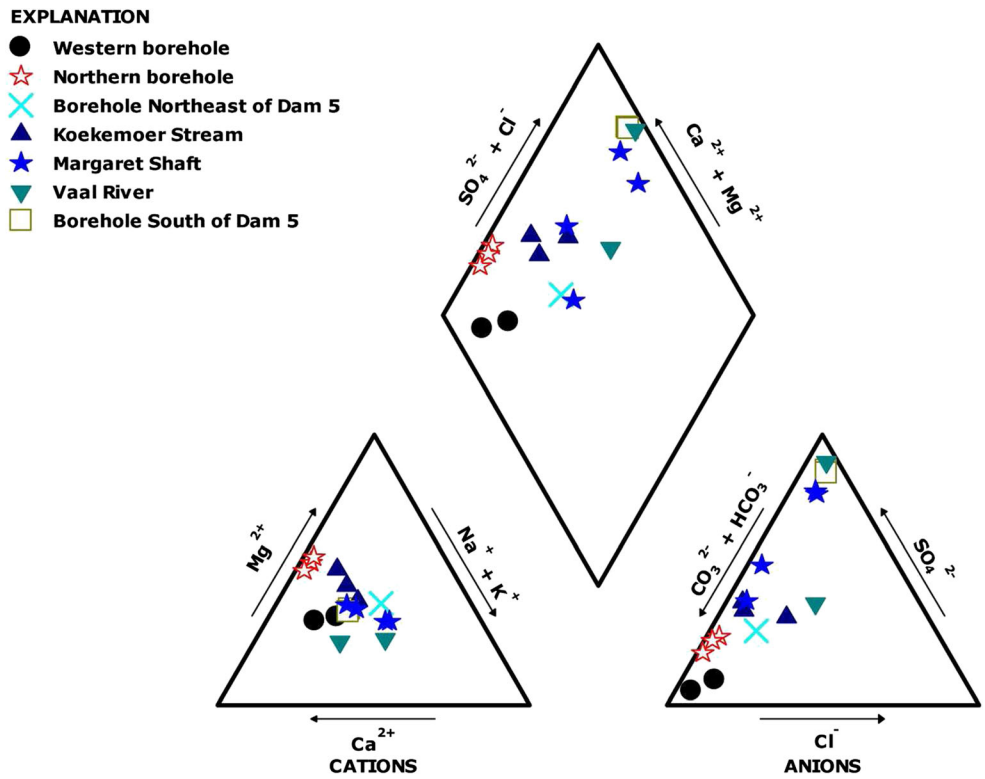

Fig. 8 Composite Piper plot of groundwater and surface-water samples using measured major ion chemistry. The three identified distinct categories include Ca–Mg–HCO_3 type, Ca–Mg–SO_4 type and a mixture of the two; Ca–Mg–HCO_3–SO_4-type waters

presumably from mine seepages, underwent extensive evaporation. On the other hand, Ca–Mg–HCO_3-type water samples were observed to have highly depleted water which did not undergo evaporation.

The majority of water intercepted at the Margaret Shaft area exclusively originates from the Ca–Mg–HCO_3-type waters supplied by the shallow permeable carbonate (dolomite) aquifer with considerable input of water from the Dam 5 seepage water of Ca–Mg–SO_4-type composition. Similar deep mine water chemistry was also reported elsewhere in Witwatersrand basin (Duane et al. 1997).

Tritium data

It has been determined that geogenic tritium (^{3}H) is negligible in natural rocks except in rocks of uranium mineralization; therefore, measurable ^{3}H in today's groundwater is of cosmogenic origin (Clark and Fritz 1997). Surface-water samples from the Vaal River, Koekemoer Stream and Dam 5 have similar values of ^{3}H (2.5±0.2 TU) and shallow groundwater from extreme south and north of Dam 5 averages 3.7±0.2 TU, whereas 1.7±0.2 TU was measured for the Margaret Shaft waters (Table 3). The ^{3}H data interpretation is consistent with the result of ESIs, i.e. that the western boreholes represent a different water type with very low ^{3}H implying older water. Qualitative assessment of relative age of recharge can be made although quantitative age determination was not possible with the current data set, as accurate calculation requires long term and profile sampling (Huang and Chen 2012). Circulation time of the shallow and deep groundwater samples was estimated to be 30 years and over 60 years, respectively, taking into account the Pretoria average rainfall ^{3}H value of 27.4 TU (IAEA 2012b).

The ESI, hydrochemical and tritium data highlight the fact that considerable influx of water is occurring into the deeper levels of Margaret Shaft from Dam 5. The water flowing into the Margaret Shaft is evidently drawn from three major sources namely: the northern shallow dolomite aquifer, the eastern dolomite aquifer and seepage

Table 3 Tritium data of selected samples in tritium units (TU), with laboratory uncertainties

Sample location	Sample ID	Tritium (TU)	Laboratory uncertainty (TU)
Western borehole	BH29	0.3	±0.2
Shaft samples			
180 m bgl	MSL-3	1.8	±0.3
350 m bgl	MSL-5	2.0	±0.3
650 m bgl	MSL-10	1.5	±0.3
950 m bgl	MSL-16	2.2	±0.3
Northern boreholes	VAN5	3.7	±0.4
	VAN7	3.8	±0.4
Koekemoer Stream	K4	2.2	±0.3
Stilfontein Bullet Factory	LW4	3.6	±0.4
Vaal River	VAAL3	2.5	±0.3
Stilfontein Dam	DAM5	2.6	±0.3

MSL Margaret Shaft level; *m bgl* meters below ground level
DAM5, *K1*, *K4*, *K5*, *VAAL1* and *VAAL2* are surface-water samples

DOI 10.1007/s10040-014-1216-z

from Dam 5, as well as the Koekemoer Stream due to short flow-path groundwater circulation. The result also confirms the presence of a water barrier west of Dam 5 along the Pilansberg dyke, perhaps limiting mixing of western shallow water with the rest of the water reaching the Margaret shaft.

Numerical modelling

Numerical modelling has been applied in many areas to understand subsurface water flow and manage water resources (Konikow and Bredehoeft 1974; Robson 1974; Gvirtzman et al. 1997; Mills et al. 2002; Leake et al. 2005). Minimization of numerical-model result uncertainties, especially uncertainties due to aquifer anisotropy and heterogeneity, has been shown unprecedented attention in recent years, leading to an understanding that it is necessary to refine flow conceptualization and recalibrate models using hydrochemical and ESI data (Swanson and Bahir 2004; Ji-Chun and Xian-Xi 2013). Effort has been made to standardize groundwater modelling in an attempt to minimize model uncertainties and to achieve improved model results albeit with controversies in a few areas (Mills et al. 2002; Swanson and Bahir 2004; Fox et al. 2011; Johnson 2010; Barnett et al. 2012).

Model domain, model discretization and model boundaries

The extent of the model area in this study is limited to only the area covered by dolomite formation, of approximately 380 km^2 (or 60 % of the entire catchment), to maintain the desired level of detail and to run the model simulation within a reasonable amount of time (Fig. 2).The model area is discretized into a grid of 100 columns and 200 rows with mesh size gridded at 91 m by 360 m because of the limited width of dykes in the E–W direction (Fig. 9). The grid size is not unreasonable as the model was designed to simulate the regional flow system.

Appropriate boundary conditions were assigned: (1) a head-dependant flow boundary (Cauchy type) was assigned along the Koekomoer Stream and the Vaal River at the southern tip of the model area; (2) a no-flow boundary was assigned around the entire model area based on location of the surface-water divide and groundwater level records. Average river conductance is assigned a value of 1 m^2/day on the basis of average aquifer thickness of 3 m and field vertical infiltration data conducted at various points along the river course.

The hydrogeological conceptual model was developed based on information obtained from ESI and hydrochemical data, several borehole logs and a 3D mine model. Based on data from aquifer tests, the anisotropic and heterogeneous dolomite aquifer has a higher average horizontal hydraulic conductivity value than the average vertical hydraulic conductivity value (Table 4). This directional heterogeneity was accounted for in model simulation by assigning a different vertical hydraulic

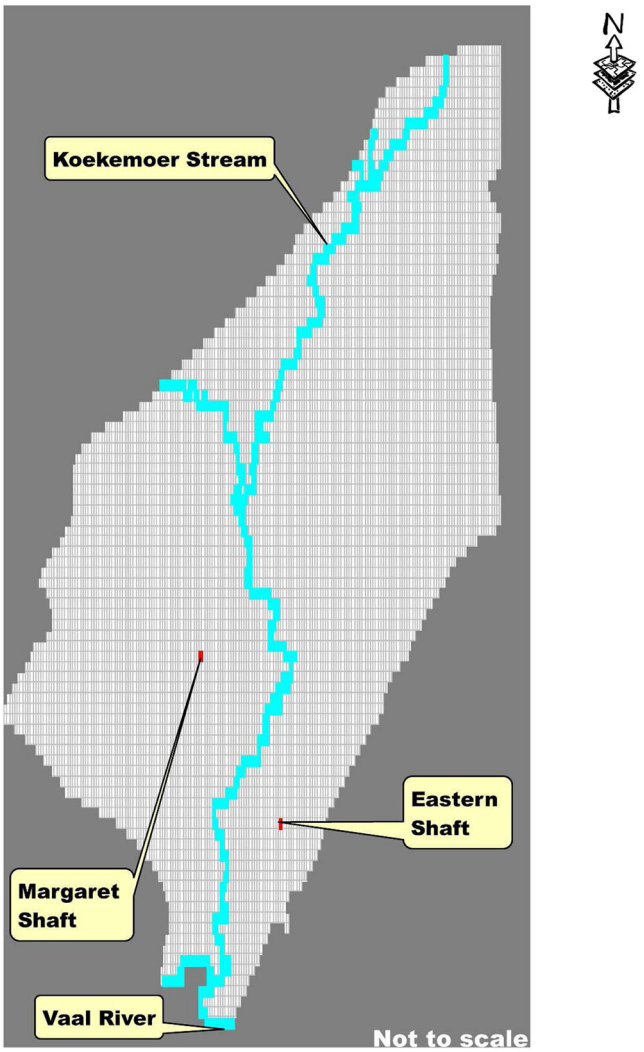

Fig. 9 Model grid of the domain with 100 columns and 200 rows

conductivity (Kv) to the local carbonate (dolomite) units, consistent with similar modelling work in the Judea carbonate in Israel (Gvirtzman et al. 1997). All relevant geological structures determined from previous work done in the area, including the kimberlite-composition dyke (N–S) and Pilanesberg dyke (NW–SE), were included in the current study and their relevant parameter values adapted for this study (Su et al. 2004).

Existing borehole information confirms the presence of weathered and karstified dolomite formation at depths 25–30 m bgl and slightly weathered and fractured to fresh massive dolomite from 30 m to maximum depth 2,500 m towards the eastern boundary of the model. The upper and lower dolomite unit together increases in thickness from the west, where the unit pinches-out, to the east where the unit is covered by younger units and reaches a thickness of about 2,500 m. However, the model area is restricted to the top 600 m, where existing field data suggest that the majority of the water flowing into the shafts comes from, and where dynamic groundwater flow is taking place. The assigned layer 1, which is the top weathered and karstified dolomite and the limited flood plains in the lower reaches

DOI 10.1007/s10040-014-1216-z

Table 4 Model initial input values based on previous and current pumping tests, as well as adapted and measured recharge estimations. Horizontal and vertical hydraulic conductivities (k_h and k_v, respectively), recharge and specific storage are also given. There are seven zones of vertical and horizontal hydraulic conductivity for the two aquifers

Model layer	Initial k_h (m/day)	Initial k_v (m/day)	Specific storage (−)	Recharge (mm/year)
Areas east of Kimberly dyke and west of Pilanesberg dyke	0.66[a]	0.02526[a]	0.002[b]	32.5
Upper dolomite (regional)	0.2524	0.02526	0.001[b]	32.5
Upper dolomite (near Kimberlite dyke)	5.5[c]	0.45[c]	0.005[c]	32.5
Upper dolomite (near Pilanesberg dyke)	0.66[c]	0.08[c]	0.001[c]	32.5
Lower dolomite (regional)	0.035[c]	0.0014[c]	0.000167[c]	-
Lower dolomite near Kimberlite dyke)	0.57[d]	0.025[d]	0.005[d]	-
Lower dolomite (near Pilanesberg dyke)	0.044[a,d]	0.0035[a,d]	0.0021[a,d]	-

[a] Veltman and Wilke (2008), unpublished data

[b] Labuschagne, Groundwater Consulting Services, unpublished data, 2007

[c] Smith and Ritzi (1993)

[d] Yager and Kappel (1998)

Pre-mine recharge value is calculated to be 28 mm/year (based on 5% of 558 mm precipitation); recharge of Dam 5 area=324.5, golf course=174.5, Buffels Tailings dam and Southern metallurgical plant return water dam area=1,423.5 mm/year. Upper dolomite (layer 1) is confined/unconfined (confined in some areas and unconfined in other areas) and bottom dolomite (layer 2) is confined. - not applicable

of the Koekemoer Stream and Vaal River, describes the field scenario reasonably well. There is also compelling evidence from a hydrocensus conducted in early 2010, that two water levels, representing two aquifers, are encountered; the top partially weathered and fractured dolomite aquifer (0–25 m bgl) and the deep dolomite aquifer (25–600 m bgl). The model is a 3D 2-layer system with appropriate hydraulic parameters assigned to the major aquifers. Initial input values used in the model are obtained from various aquifer test data, infiltration tests, and chloride and tritium measurements (Table 4).

Storativity values were adapted from current and earlier aquifer tests for the entire upper dolomite aquifer as well as from a report compiled on a similar formation just south of the Vaal River (Labuschagne, Groundwater Consulting Services, unpublished data, 2007). Therefore, knowing the average thickness of the formation in the local area, specific storage values were estimated to be ranging from 0.0001 to 0.005 (Table 4).

Initial conditions

Aquifer hydraulic conductivity was assigned based on results obtained from aquifer tests in the dolomite aquifer, which was subdivided into areas situated west and east of the two dykes (Kimberlite and Pilanesberg). A total of 130 boreholes, situated in the vicinity of the shafts, were used as observation points. The steady-state pre-mining head distribution, calibrated with measured hydraulic heads far away from the current dewatering and mining operations, was taken as initial head for the transient simulation.

Pre-mining recharge was calculated to be 5 % (28 mm) of the mean annual precipitation (558 mm/year) using 24 years of rainfall data (Fig. 10; T. Else of Margaret Water Company, personal communication, 2010). Recharge in areas along river channels was estimated at 44.6 mm/year, which is slightly different from an earlier estimation by Hodgson et al. (2001). Field infiltration data were used to estimate the induced recharge value from tailings dams, evaporation dams, Stilfontein Golf course,

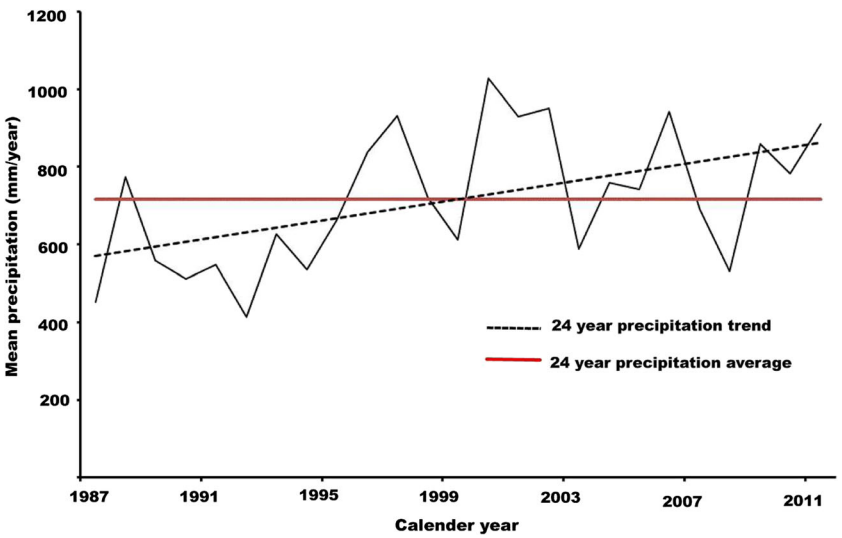

Fig. 10 Mean annual precipitation between 1988 and 2011; the mean of the 24 years of data is shown as a *horizontal line* at 710 mm/year

South Metallurgical Plant and return water dams (Table 4). Relevant additional aquifer parameters, including transmissivity, storage coefficient and effective porosity, were acquired from current and previous aquifer tests.

Records from the major pumping shafts (Margaret Shaft and Eastern Shaft) show that pumping rate changes from time to time for various reasons and as a result, the simulation was carried out with transient state. The simulation was subdivided into seven stress periods ranging from 100 days up to 100 years. The specific stress periods were chosen on the basis of 12 years of pumping rate data and are detailed in Table 5, which also shows the pumping rates used for the seven stress periods. A decreasing trend of pumping rate is the reason for using the 10-year average for simulating the long-term pumping scenario. There are no subsidence and compaction observation data and, therefore, no such aquifer property was incorporated.

Sensitivity testing

Parameter sensitivity tests were conducted iteratively using forward simulation to test the influence of change in magnitude of input parameters on the simulation results of the groundwater model (Gedeon and Mallants 2012). To this effect, sensitivity tests were conducted using river conductance (streambed leakance) ranging in values from 0.02 to 200 m^2/day. It turned out that streambed leakance was insensitive when river conductance exceeds 4 m^2/day. Specific storage was categorized as type-IV sensitivity because the parameter modifies model result as well as the magnitude of simulation residual error significantly. Horizontal hydraulic conductivity of the upper aquifer exhibits high sensitivity to change, resulting in a change of the model outcome and the simulation residual error. The recharge parameter is type-IV sensitive, in that a slight change causes drastic change in model outcome as well as simulation residual error. Similarly, recharge is a parameter that causes non-convergence when the transient simulation causes dry cells within the domain.

Model calibration

Non-uniqueness is constrained by reducing the number of parameters or by regularization, which is a way of ensuring that parameter estimates do not deviate from initial estimates that are considered to be reasonable (Leake et al. 2005). Steady-state groundwater-head simulation data were calibrated using hydraulic head data sufficiently distant from the influence of dewatering at the model domain margins and outside the model boundary because hydraulic head measurements of pre-mining conditions do not exist; these conditions were taken to be a substitute for the pre-mining state, before 1949. Automated parameter estimation was used to perform inverse modelling and to allow optimized values of vertical and horizontal hydraulic conductivities of the two aquifers to be calculated. The PEST module iteratively calculated values until the lowest root mean squared (RMS) error was achieved. The final pre-mining groundwater head distribution, representing minimum RMS error between steady-state model simulated and measured data, was plotted (Fig. 11). RMS error of the 43 boreholes, out of the 130 calculated between the simulated and measured hydraulic head data, is 28.9 while standard deviation is 30.8. Additional data regarding model-generated and measured head can be found in the ESM.

Inverse modelling was undertaken to determine optimum recharge value using the calculated hydraulic conductivity values and measured groundwater heads. Mining conditions (increased recharge below tailings dams and Stilfontein Golf Course, as well as pumping conditions at Margaret and Eastern shafts) were applied to compare measured and simulated head distributions. The process was repeated many times iteratively until a close match was obtained. It is seen in Fig. 12 that plots of observed and calculated head data for the transient simulation display an initial gap perhaps due to numerical instability at the beginning of the simulation; however, after the first two stress periods, the graph exhibits a close fit and clearly corresponds to the dewatering and induced recharge events.

Model validation was affirmed with reasonable water-balance calculation, which shows the inflow mass is very close to what is flowing out of the system (Table 6). The stress period 3 water mass balance data exclusively incorporates measured values such as well abstraction rate and is consistent with similar water balance studies compiled elsewhere in the region (Ogola et al. 2011).

Table 5 Pumping rates, time steps, and stress-period durations used in transient simulation and zone of influence sizes. Pumping rates were determined on the basis of measured pumping data

Stress period	Duration (days)	No. of time steps	Pump rate (m^3/day)	Width×depth (Margaret Shaft)[a]	Width×depth (Eastern Shaft)[a]
1	100	5	53,000	-	-
2	365 (1 year)	10	38,718	-	-
3	1,460 (4 years)	15	26,970	200 m×200 m	100 m×30 m
4	2,190 (6 years)	20	45,955	-	-
5	3,650 (10 years)	25	37,213	1.8 km×250 m (layer 1) 1.4 km×270 m (layer 2)	430×30 m (layer 1) 500 m×60 m (layer 2)
6	10,950 (30 years)	35	37,213	-	-
7	36,500 (100 years)	50	37,213	1.9 km (E–W) and 2.5 km (N–S)×500 m	500 m×100 m

[a] Refers to estimated width of the cone-of-depression expressed in diameter of a roughly circular area of influence, and depth of the cone-of-depression as the maximum drawdown created at the shaft due to pumping

 DOI 10.1007/s10040-014-1216-z

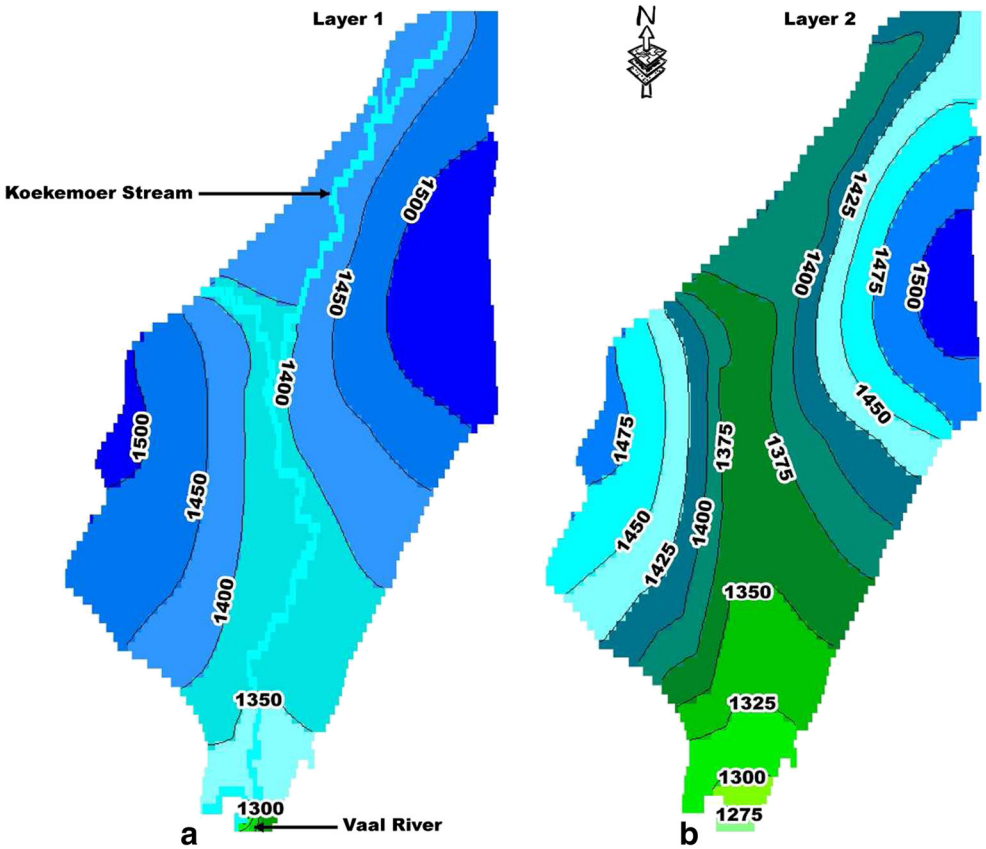

Fig. 11 Steady-state groundwater-head-simulation results for the pre-mining scenario represented by years before 1949 in **a** layer 1 and **b** layer 2. The contour units are groundwater head elevations in meters above mean sea level

Given the limitations associated with model discretization such as uncertainties in spatial distribution of hydraulic properties as well as interpolations (in space and time) and the related assumptions regarding

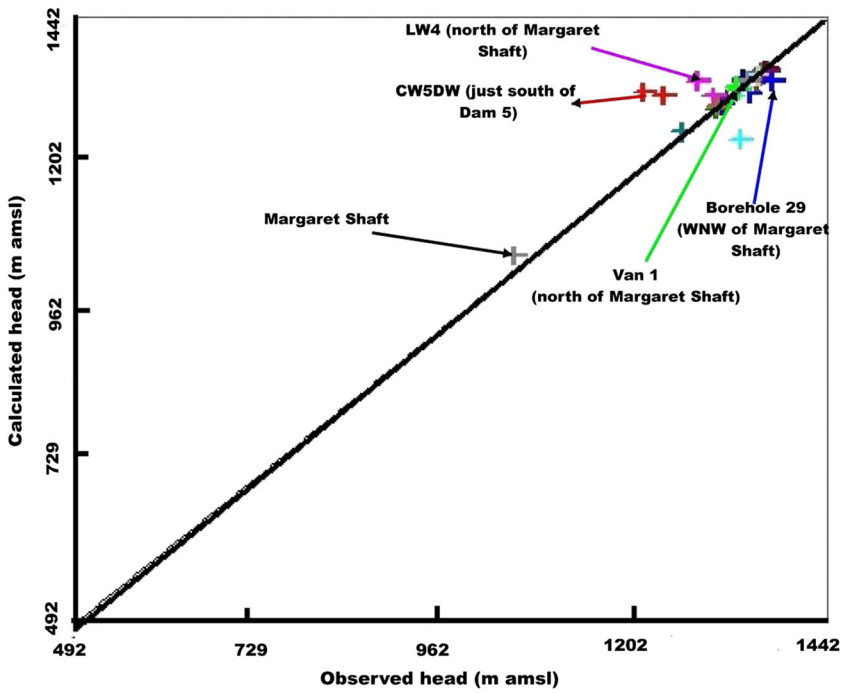

Fig. 12 Transient-state (stress period 3) groundwater head simulation compared with measured groundwater-level elevation for Margaret Shaft and surrounding boreholes. *m amsl* meters above mean sea level

 DOI 10.1007/s10040-014-1216-z

Table 6 Model-generated water budget, calculated for the entire domain. The discrepancies are in percent between input and outflow[c]

Flow term	Inflow[a] (m^3/day)	Outflow[b] (m^3/day)	Inflow–Outflow (m^3/day)
Storage	131,903.5	111,451.8	20,425.7
Well abstraction	0.0	59,000.0	59,000.0
Recharge	40,280.9	0.0	40,280.9
River leakage	365.4	2,135.6	−1,770.1
SUM	172,549.8	172,587.4	−37.6

[a] Inflow refers to the volume of water entering into the domain (model area)

[b] Outflow shows the volume of water leaving the model area

[c] Discrepancy is an indicator of model accuracy as it measures the difference between the volume of water entering and leaving the model domain. The lower the discrepancy, the higher the model credibility. Discrepancy (0.02 %) was calculated as: **Discrepancy** = $\left[\frac{\text{Inflow}}{\text{Inflow}-\text{Outflow}}\right] \times 100$ %

underground tunnelling, heterogeneity and anisotropy appear not to significantly affect the reliability of the simulation.

Model results

Cognisant of the fact that the aquifer has been undergoing considerable stress since mining commenced in the early 1900s, reasonable steady-state pre-mining head distribution was achieved and used as initial head distribution for the transient simulation under mining conditions. It is relevant to highlight that extensive efforts were made to incorporate critical hydrologic information into the numerical model for improved prediction of future consequences of the pumping and identify the source of water flowing into the shafts.

A transient model run was executed on the basis of seven stress periods of up to 100 years starting from day-100 based on measured pump rate data of the two main shafts. A number of runs were carried out to understand the aquifer response to various scenarios pertaining to dewatering conditions and induced recharge from local surface-water sources.

The model run after 1,460 days (stress period 3) exhibits a cone-of-depression around Margaret and Eastern shafts in layer 1 as well as layer 2 creating local flows (Table 5). It is also apparent that 4 years of dewatering causes modest change from the 100-days (stress period 1) scenario (not shown) except that the various induced-recharge islands do not appear in the fourth-year stress period in layer 1 (upper dolomite). The deeper and narrower area of influence in the bottom dolomite is explained by diminished hydraulic conductivity and specific capacity of the solid dolomite. A similar trend of deeper and narrower zone influence is also observed in the Eastern Shaft dewatering area.

On the other hand, dewatering the top dolomite aquifer for 10 years (stress period 5) with average rate slightly higher than 37,000 m^3/day modifies the extent of the cone-of-depression around Margaret and Eastern shafts (Fig. 13; Table 5). According to the model result of stress 5, if seepage from Dam 5 is stopped or substantially

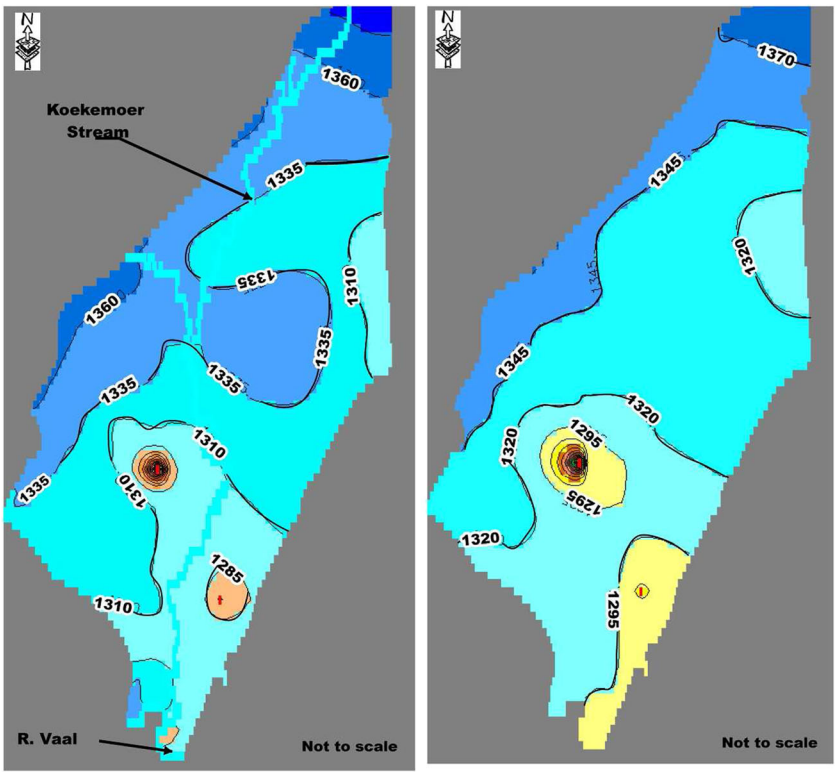

Fig. 13 Model run results of stress period 5 (10 years with 25 steps) in **a** layer 1 and **b** layer 2. Resulting transient hydraulic heads are displayed in m amsl

 DOI 10.1007/s10040-014-1216-z

reduced due to decommissioning, the shallow farm boreholes in the north would dry up due to fast northern expansion of the cone-of-depression after the 10-year pumping.

The 100-year stress period (stress period 7) in the top dolomite shows that the shape of area subject to the dewatering is extensively modified from stress period 5 (Table 5), suggesting that three-quarters of the top dolomite is dewatered completely by the pumping. A slightly modified shape and depth of zone of influence was created in the bottom dolomite (Fig. 14b). It is interesting to note that extended periods of pumping and induced recharge also create isolated zones of high groundwater head especially south of the South Metallurgical Plant and Buffels tailings dam in the top dolomite aquifer (Fig. 14a).

The combined rate of pumping at the two shafts is significant enough to create a wide radius of influence but not big enough to be similar in magnitude than previously reported by Dewandel et al. (2006), indicating that the aquifer transmissivity of the bottom dolomite may have been over estimated. The widest cone-of-depression in the area generated from the model simulation is about half of what was reported in a previous study by Dewandel et al. (2006).The result also underscores the considerable influence of Kimberlite Dyke, which conduits water at a much faster rate than the surrounding formation. Moreover, the result shows that the recharge from Dam 5 and surrounding surface water is substantial enough to limit the cone of depression from expanding northward.

Model result implications

According to Veltman and Wilke—Digby Wells Associates, unpublished data (2008)—geophysical data inferred that a hydraulic barrier could exist within the dolomitic aquifer west, north and south of Dam 5. The geophysical data confirm the existence of an impermeable dyke just west of Dam 5 consistent with groundwater hydrochemical and ESI results. However, the measured hydraulic head distributions do not indicate the presence of any barrier on groundwater movement. The result of the present study does not support the view that there is a no-flow boundary north and south of Dam 5.

The present numerical groundwater flow model postulates that groundwater captured at Margaret Shaft originates from a much narrower area than previously thought, with considerable seepages from Dam 5 and the dolomite aquifer, especially along the permeable zones in the proximity of the Kimberlite Dyke.

Possible decommissioning of Dam 5 would reduce the amount of induced recharge and create a scenario whereby

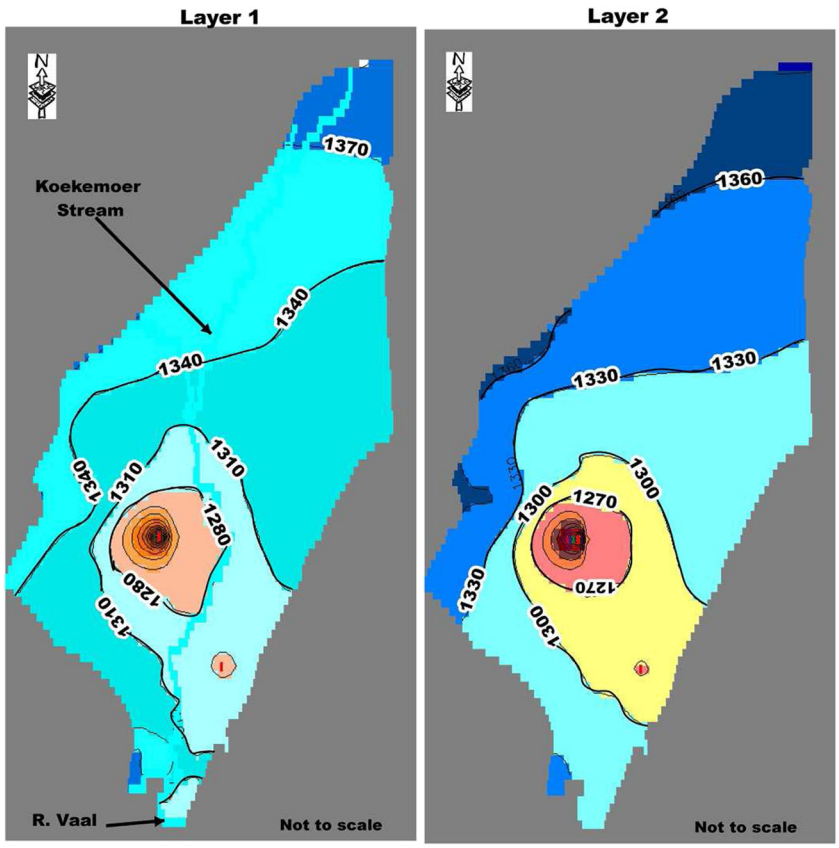

Fig. 14 Model run results of stress period 7 (100 years with 50 steps) in **a** layer 1 and **b** layer 2. Resulting transient hydraulic heads are displayed in m amsl

 DOI 10.1007/s10040-014-1216-z

the cone-of-depression rapidly grows more towards the north than is predicted by the model. The implications of the cessation of Dam 5 as a central tailings dam could be even more profound, in that the shallow farm boreholes north of Dam 5 would eventually dry up.

Model limitations

The major limitation of the model is the extent to which the vertical and horizontal hydraulic conductivity zones represent the real field situation in the top highly fractured, weathered and karstified dolomite aquifer as well as the bottom slightly fractured dolomite unit. Moreover, the homogeneity of the individual zones is also an assumption that perhaps increases the level of model uncertainty.

A small portion (1–2 %) of the model domain underwent extensive underground mining, which would obviously create mined-out areas that present small zones of high permeability. Although the majority of the stoppings and network of tunnels may have collapsed, the real value of aquifer parameters (storage coefficient and transmissivity) may not accurately be defined. The model domain boundary is delimited entirely on the basis of the surface-water catchment and the assumed no-flow boundaries could be compromised due to limited cross-boundary flows into the model area especially in the northwest portion of the model where a part of the catchment was disregarded because of the pinching-out of the dolomite formation.

Conclusions

ESI data confirm that up to 50 % of the water in the Margaret shaft originates from seepage of Dam 5, whereas the rest of the water comes from the shallow carbonate aquifer as well as direct recharge from precipitation. Hydrochemical data of the deep shaft water samples demonstrate a signature of Ca–Mg–SO_4-type water mixing with the natural Ca–Mg–HCO_3 water types. Isotopically depleted water samples correspond to Ca–Mg–HCO_3, whereas samples relatively enriched with stable isotopes are characterized by Ca–Mg–SO_4-type waters. Furthermore, the tritium data of the shaft water encountered at deep levels of up to 950 m bgl exhibit recent recharge, suggesting seepage from Dam 5 and shallow groundwater. Hydrochemical and ESI data improved the conceptual understanding of the local groundwater flow system, which subsequently helped the interpretation of the numerical modelling.

It is concluded that the reported increase in fissure water is consistent with the increased amount of waste water produced by substantial reprocessing activities of old tailings materials in the years spanning between 2006 and 2009, as well as increase in average annual precipitation over the region in the last decade.

The present findings suggest that the source of water at the shaft is a much narrower area than previously reported and that the contribution of seepage water from Dam 5 is significant enough to limit northerly expansion of the cone-of-depression.

The shallow farm boreholes in the northern area would dry up within approximately 10 years of pumping at the shaft as a consequence of cessation of Dam 5 being used as a central tailings dam, due to fast northern expansion of the cone-of-depression.

The results underscore the fact that the integrated mine-water management implemented at KOSH area mines is proven to be cost effective by capturing surface water at a relatively shallow depth before the mine water finds its way into the deeper levels of downstream mines.

Acknowledgements The authors would like to acknowledge Dr. Robel Gebrekristos of Digby Wells Associates for his contribution in improving the manuscript and for several hours of discussion, Trevor Else of Margaret Water Company, Robert White of Basic Bed Rock Strata Company, Charles Human and Joel Mallan of AngloGold Ashanti Mine, Ugo Nzota and Thato Kgari of the Council for Geoscience, Yazeed van Wyk of the University of Pretoria, Fortress Netili of the International Water Research Institute, and the Council for Geoscience Organization.

Reference

Abiye TA, Mengistu H, Demlie MB (2011) Groundwater resource in the crystalline rocks of the Johannesburg area, South Africa. J Water Resour Prot (JWARP) 3:199–211

Aravena R (1995) Isotope hydrology and geochemistry of northern Chile groundwaters. Bull Inst Fr Estudes Andines 24(3):495–503

Barnett B, Townley LR, Post V, Evans RE, Hunt RJ, Peeters L, Richardson S, Werner AD, Knapton A, Bronkay A (2012) Australian groundwater modelling guidelines. Waterlines 82, pp 1–203

Chiang W (2005) 3D-Groundwater modelling with PMWIN, 2nd edn. Springer, Heidelberg, 397 pp

Clark I, Fritz P (1997) Environmental isotopes in hydrogeology. Lewis, New York, 328 pp

Craig H (1961) Isotopic variations in meteoric waters. Sci 133(3465):1072–1703

Dewandel B, Lachassagne P, Wyns R, Maréchal JC, Krishnamurthy NS (2006) A generalized 3-D geological and hydrogeological conceptual model of granite aquifers controlled by single or multiphase weathering. J Hydrol 330:260–284

Dotsika E, Lykoudis S, Poutoukis D (2010) Spatial distribution of the isotopic composition of precipitation and spring water in Greece. Glob Planet Change 71:141–149

Duane MJ, Pigozzi G, Harris C (1997) Geochemistry of some deep gold mine waters from the western portion of the Witwatersrand Basin, South Africa. J Afr Earth Sci 24(1/2):105–123

Dept. of Mineral and Energy Affairs (1986) Geological Map of West Rand at 1:250,000 scale. Department of Mineral and Energy Affairs, Government Printer, Pretoria

DWA (Department of Water Affairs) Report (2006) Development of a catchment management strategy for the Schoonspruit and Koekemoerspruit Catchments in the middle Vaal management area. Report No. 16/2/7, vol 6, DWA, Pretoria

Eriksson PG, Altermann W, Hartzer FJ (2006) The Transvaal supergroup and its precursors. In: Johnson MR, Anhaeusser CR, Thomas RJ (eds) The geology of South Africa. Geological Society of South Africa, Johannesburg, pp 237–260

Farlin J, Lai CT, Yoshimur K (2013) Influence of synoptic weather events on the isotopic composition of atmospheric moisture in a coastal city of the western United States. Water Resour Res 49:1–12
Fox AG, Heeren MD, Kizer AM (2011) Evaluation of a stream aquifer analysis test for deriving reach-scale streambed conductance. Trans Am Soc Agric Biol Eng (ASABE) 54(2):473–479
Gat JR, Mook WG, Meijer HAJ (2001) Observed isotope effects in precipitation, chapt 4. In: Moor WG (ed) Environmental isotopes in the hydrological cycle: principles and applications, vol 2, no. 39. UNESCO, Paris, pp 43–59
Gedeon M, Mallants D (2012) Sensitivity of analyses of a combined groundwater flow and solute transport model using local-grid refinement: a case history. Math Geosci 44:881–889
Gibson JJ, Edwards TWD, Bursey GG (1993) Estimating evaporation using stable isotopes: quantitative results and sensitivity analysis for two catchments in northern Canada. Nord Hydrol 24(1993):79–94
Gvirtzman H, Garven G, Gvirtzman G (1997) Hydrogeological modelling of the saline hot springs at the Sea of Galilee, Israel. Water Resour Res 33(5):913–926
Harbaugh AW, Banta ER, Hill MC, McDonald MK (2000) MODFLOW-2000. The U.S. Geological Survey modular ground-water model: user guide to modularization concepts and the ground-water flow process. US Geol Surv Open-File Rep
Harris C, Burgers C, Miller J, Rawoot F (2010) Oxygen- and hydrogen-isotope record of Cape Town rainfall from 1996 to 2008, and its application to recharge studies of table mountain groundwater, South Africa. South Afr J Geol 113:33–56
Hodgson FDI, Usher BH, Scott R, Zeelie S, Cruywagen LM, de Necker E (2001) Prediction techniques and preventative measures relating to the post-operational impact of underground mines on the quality and quantity of groundwater resources. Water Research Commission Report no. 699/1/01. Water Research Commission, Pretoria, South Africa
Huang P, Chen J (2012) Recharge sources and hydrogeochemical evolution of groundwater in the coal-mining district of Jiazuo, China. Hydrogeol J 20:739–754
International Atomic Energy Agency (IAEA) (2012b) The Global Network of Isotopes in Precipitation (GNIP) http://iaea.org/water. Accessed 10 December 2012
Ji-Chun W, Xian-Xi Z (2013) Review of the uncertainty of groundwater numerical simulation. Chin Sci Bull 58(25):3044–3052
Johnson J (2010) Framework to effectively quantify and communicate groundwater model uncertainty to management and clients. US Department of Interior Bureau of Reclamation, Pacific NW Regional Office, Boise, ID
Kafri U, Foster MBJ (1989) Hydrogeology of the Malmani Dolomite in the Klip River and Natalspruit basins, South Africa. Environ Geol 13(2):153–166
Keating HE, Doherty J, Vrugt AJ, Kang Q (2010) Optimization and uncertainty assessment of strongly non-linear groundwater models with high parameter dimensionality. Water Resour Res 46:1–13
Konikow LF, Bredehoeft JD (1974) Modelling flow and chemical quality changes in an irrigated stream aquifer system. Water Res 10(3):546–562
Larsen D, Swihart GH, Xiao Y (2001) Hydrochemistry and isotope composition of springs in the Tecopa basin, southeastern California, USA. Chem Geol 179:17–35
Leake SA, Hoffmann JP, Dickinson JE (2005) Numerical groundwater change model of the C Aquifer and effects of groundwater withdrawals on stream depletion in elected reaches of Clear Creek, Chevelon Creek, and the Little Colorado River, northeastern Arizona, US Geol Surv Sci Invest Rep 2005–5277
Lee JE, Fung I (2007) Changing partitioning of vapour source between transported vapour and local evaporation events. Hydrol Proc 22:1–8
Mazor E (1997) Chemical and isotopic groundwater hydrology. Dekker, New York, 413 pp
McCarthy TS (2006) The Witwatersrand Supergroup. In: CR Anhaeusser, RJ Thomas, MR Johnson (eds) The geology of South Africa. Geol Soc SA, Johannesburg, pp 155–186
Mills PC, Nazimek JE, Halford KJ, Yeskis DJ (2002) Hydrogeology and simulation of ground-water flow in the aquifers underlying Belvidere, Illinois. US Geol Surv Water Resour Invest Rep 01–4100
Naickera K, Cukrowskaa E, McCarthy TS (2003) Acid mine drainage arising from gold mining activity in Johannesburg, South Africa and environs. Environ Pollut 122:29–40
Ogola J, Maiyana B, Yibas B (2011) Water balance determination of mine residue deposits: case studies in the Witwatersrand Basin, South Africa. In: Proceedings of the 11th Mine Water Association Congress. Mine water: managing the challenges. Aachen, Germany, 2011, pp 615– 618
Poage MN, Chamberlain CP (2001) Empirical relationships between elevation and the stable isotope composition of precipitation and surface water: considerations for studies of paleo-elevation change. Am J Sci 301:1–15
Prinsloo MJ (2007) Explanation for 1:250,000 geological map series of South Africa and Namibia. Geol Surv South Afr 3022
Pulido-Bosch A, Vallejos A, Martin-Rosales W, Calvache ML (1997) Contribution of environmental isotopes to the understanding of complex hydrologic systems: a case study—Sierra De Gador, SE Spain. Earth Surf Proc Landf 22:1157–1168
Robson S (1974) Feasibility of digital water quality modelling illustrated by application of Barstow, California. US Geol Surv Water Resour Invest Rep 46–73
Schimmelmann A, DeNiro MJ (1993) Preparation of organic and water hydrogen for stable isotope analysis: effects due to reaction vessels and zinc. Anal Chem 65:789–792
Schofielda S, Jankowski J (2004) Hydrochemistry and isotopic composition of Na–HCO3-rich groundwaters from the Ballimore region, central New South Wales, Australia. Chem Geol 211:111–134
Smith RT, Ritzi RW (1993) Designing a nitrate monitoring program in a heterogeneous carbonate aquifer. Ground Water 31(4):576–584
Socki RA, Karlsson HR, Gibson EK (1992) Extraction technique for the determination of oxygen-18 in water using pre-evacuated glass vials. Anal Chem 64:829–831
South African Committee for Stratigraphy (SACS) 1980 Stratigraphy of South Africa, part 1. Government Printer, Pretoria
Su GW, Jasperse J, Seymour D, Constantz J (2004) Estimation of hydraulic conductivity in an alluvial system using temperatures. Ground Water 4(6):890–901
Swanson SK, Bahir JM (2004) Analytical and numerical models to explain steady rates of spring flow. Ground Water 4(5):747–759
Tessema A, Mengistu H, Chirenje E, Abiye TA, Demlie MB (2012) The relationship between lineaments and borehole yield in North West Province, South Africa: results from geophysical studies. Hydrogeol J 20:351–368
Van Niekerk HJ, van der Walt IJ (2006) Dewatering of the Far West Rand dolomitic area by gold mining activities and subsequent ground instability. Land Degrad Dev 17:441–452
Veltman S, Wilke AR (2008) Groundwater flow mechanisms at Margaret shaft, KOSH Gold mining area. 2008 International Mine Water Conference Proceedings. http://www.imwa.info/docs/imwa_2008/IMWA2008_188_Veltman.pdf. Accessed 11 December 2012
Voss CI (2011a) Groundwater modelling fantasies, part 1: adrift in the details. Hydrogeol J 19:1281–1284
Voss CI (2011b) Groundwater modelling fantasies, part 2: down to earth. Hydrogeol J 19:1455–1458
Winde F, van der Walt IJ (2004) The significance of groundwater–stream interactions and fluctuating stream chemistry on waterborne uranium contamination of streams: a case study from a gold mining site in South Africa. J Hydrol 287:178–196
Yager RM, Kappel WM (1998) Infiltration and hydraulic connections from the Niagara River to a fractured dolomite aquifer in Niagara Falls, New York. J Hydrol 206:84–97